# Development and Characterization of Metal-Salt-Doped Polyvinyl Alcohol/Polyaniline Nanocomposite Films with Enhanced Antibacterial Properties

**Raied A. Omar**
**Mohammed G. Hammed**

Department of Physics,
College of Science,
University of Anbar,
Anbar, IRAQ


This study presents the preparation and analysis of homogeneous polyvinyl alcohol (PVA) and polyaniline (PANI) blends in a 50:50 ratio, doped with $CuCl_3$ and $AgNO_3$ salts. Thin films of these nanocomposites were fabricated using the casting method. Structural, morphological, and antibacterial properties were characterized. XRD revealed partial crystallinity with new peaks for AgO and CuO due to oxidation. FE-SEM transformed from smooth to rough, porous surfaces in the doped composites. FTIR confirmed molecular interactions and successful nanoparticle integration. Antibacterial tests showed significant inhibition zones against Staphylococcus aureus and Escherichia coli, particularly in $AgNO_3$-doped samples.

***Keywords*:** Polyaniline; Polyvinyl alcohol; Nanocomposites; Antibacterial activity
**Received:** 25 July 2024; **Revised:** 03 October 2024; **Accepted:** 10 October 2024

## 1. Introduction

Polymer nanocomposites have emerged as a significant research area due to their enhanced mechanical, thermal, and antibacterial properties, critical for various applications, especially in the biomedical field [1]. Among these polymers, polyvinyl alcohol (PVA) and polyaniline (PANI) stand out for their unique and advantageous properties. PVA is known for its excellent chemical resistance, film-forming capability, and biodegradability, making it suitable for various applications. On the other hand, PANI is appreciated for its electrical conductivity, environmental stability, and easy synthesis [2].

Recently, polymer blends have become increasingly important in various industries owing to their versatile final properties, ease of production, and lightweight nature. The growing interest in polymer blends stems from their ability to combine the distinct characteristics of different polymers, leading to materials with enhanced properties tailored for specific applications [3]. The incorporation of metallic nanoparticles into polymer matrices has garnered significant attention owing to their additional functionalities, such as enhanced mechanical strength and excellent antibacterial properties [4]. Metal nanoparticles like silver (Ag) and copper (Cu) are mainly recognized for their strong antibacterial properties, which are particularly effective in medical and healthcare applications [5]. Integrating these nanoparticles with polymers such as PVA and PANI can significantly enhance their characteristics, broadening their potential applications [6]. These nanocomposites have vast potential applications, particularly in developing antimicrobial coatings and materials that prevent bacterial growth on surfaces [7]. This is particularly critical in clinical settings where bacterial infections and antibiotic resistance are increasingly concerning [8]. Understanding the interactions between the polymer matrix and metal nanoparticles is essential for optimizing these materials [9].

In this study, nanocomposite films based on PVA and PANI reinforced with metal salts such as $CuCl_3$ and $AgNO_3$ were synthesized using the casting method. The preparation process involved the preparation of homogeneous solutions of PVA. Copolymer, followed by the incorporation of the salts. The structural, morphological, and optical properties of the resulting nanocomposites were characterized using advanced techniques.

## 2. Experimental Part

A solution of polyvinyl alcohol (PVA) was prepared by dissolving 1 g of PVA in 30 mL of distilled water, stirring at 90°C for 3 hours using a magnetic stirrer. Similarly, 1 g of polyaniline (PANI) was dissolved in 30 mL of distilled water and stirred at 30°C for 2 hours. For the metal salts, 1 g of $CuCl_3$ was dissolved in 30 mL of distilled water and stirred at 30°C for 2 hours, while 1 g of $AgNO_3$ was dissolved in 30 mL of distilled water and stirred at 45°C for 3 hours.

After preparing the individual solutions, a homogeneous mixture was obtained by combining PVA and PANI in a 50:50 ratio. This blend was stirred for 30 min at 27 °C using a magnetic stirrer. Subsequently, 10 wt.% of $CuCl_3$ and 10 wt.% of $AgNO_3$ nanoparticles were separately added to the polymer blend. Each nanoparticle-polymer mixture was stirred for 30 min under the same conditions, as summarized in table (1).

  

**Table (1) Composition of the blend and nanocomposite samples prepared in this study**

| Sample | Blend | wt.% | Additive |
|---|---|---|---|
| S1 | PANI+PVA | 50:50 | - |
| S2 | PANI+PVA | 50:50 | 10 wt.% $AgNO_3$ |
| S3 | PANI+PVA | 50:50 | 10 wt.% $CuCl_3$ |

The cleaned and dried glass substrates were placed on a horizontal surface to ensure an even distribution of the polymer blends, and the measurements were performed using a balance scale. Thin films of mixtures containing $CuCl_3$/$AgNO_3$ nanoparticles were prepared using the casting method. The slides were covered with glass to prevent contamination and left at room temperature for 4 days to form homogeneous thin films. The thickness of the films was measured using a micrometer, which was about 100 µm.

The structural characteristics and antibacterial activities of the polymer blends and nanocomposite samples were analyzed using various analytical techniques. The structural properties were examined using Shimadzu XRD-6000 X-ray diffraction system. Surface morphology was analyzed using a high-resolution Inspect F-50 Field-Emission Scanning Electron Microscope (FE-SEM). Fourier-transform infrared (FTIR) analysis was performed using a Bruker FTIR instrument, Tensor-27.

To ensure reliable results, the antibacterial activity test was conducted in triplicate for each sample using the diffusion well method on Mueller-Hinton agar plates. The plates were incubated for 24 hours, and the average diameter of the inhibition zone was calculated to assess antibacterial activity.

## 3. Results and Discussion

XRD was used to study the crystalline structures of the copolymers and nanocomposites. The diffraction pattern was analyzed to determine the degree of crystallinity and the size of the crystalline regions. Figure (1) shows the XRD patterns of the synthesized PANI:PVA and PANI:PVA/$AgNO_3$ composite films. It can be observed that the broad peak around 2θ = 22.12° for the PANI:PVA sample indicates the partial crystallinity of the copolymer blend corresponding to both polymers PVA and PANI [10]. Polymers typically exhibit a semi-crystalline structure, meaning they have regions of both crystalline and amorphous phases. The partial crystallinity significantly influences the mechanical, thermal, and chemical properties. Crystalline regions resulted from ordered areas where polymer chains align in a regular, repeating pattern. Crystalline regions are responsible for the strength, rigidity, and melting point of polymers. The amorphous regions as the polymer chains arranged randomly, which contribute to the polymer flexibility. There are many factors that affect the degree of crystallinity of a polymer, such as the polymerization method [11].

The XRD pattern of PANI:PVA reinforced with 10% $AgNO_3$ shows new peaks at 20.28°, 21.61°, 24.12°, 29.63°, 31.99°, and 32.57° corresponding to $AgNO_3$ structure according to JCPDS card no. 01-084-0713, and additional peaks corresponding to the AgO structure according to JCPDS card no. 96-900-8963.

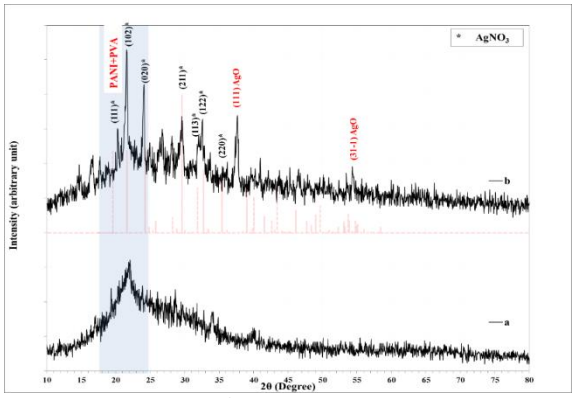


**Fig. (1) XRD patterns of (a) the PANI:PVA blend and (b) its composite reinforced with $AgNO_3$**

Bragg's equation was employed to determine the inter-planar spacing ($d_{hkl}$) as follows [12]:

$$n\lambda = 2dsin\theta \quad (1)$$

Here, $n$ is the diffraction order, $\lambda$ is the wavelength of the x-ray, and $\theta$ is the angle of diffraction

While Scherrer's formula was utilized to calculate the crystallite size ($D$) as follows [13]:

$$D(nm) = \frac{0.94\,\lambda}{\beta.cos(\theta)} \quad (2)$$

where $\beta$ is the full-width at half maximum (FWHM) of the diffraction peak. Table (2) lists the details of diffraction parameters.

The PANI:PVA/$CuCl_3$ nanocomposite was analyzed by XRD and compared with the XRD pattern of the PANI:PVA blend, as shown in Fig. (2). Critical parameters from the XRD analysis include the $d_{hkl}$ spacing, which was determined according to the Bragg's angle (2θ), and crystallite size ($D$), which was determined based on the FWHM of the diffraction peaks. These parameters were used to determine the crystallinity by matching with standard diffraction lines. The XRD pattern of PANI:PVA after reinforcement with 10% $CuCl_3$ shows diffraction peaks located at Bragg's angles of 2θ= 35.3166°, 38.8270°, 45.0744°, 48.9120°, 57.8071°, and 61.6447°, corresponding to the crystallite planes $(1\bar{1}1)$, (111), $(\bar{1}12)$, $(20\bar{2})$, (202), and $(\bar{1}13)$. Additionally, of monoclinic CuO structure according to JCPDS card No. 96-101-1195, as shown in table (2), confirms the successful integration of oxide form (CuO) into the copolymer matrix [14].

  

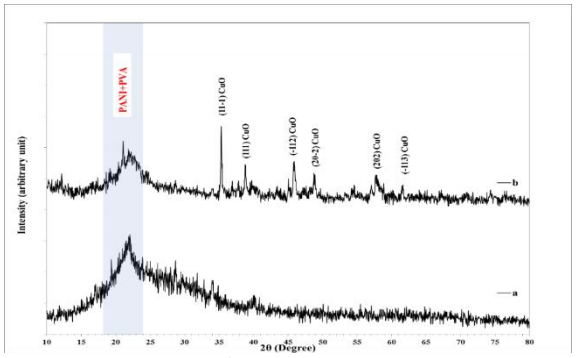


**Fig. (2) XRD patterns of (a) the PANI:PVA blend and (b) its composite reinforced with $CuCl_3$**

Field-emission scanning electron microscopy (FE-SEM) provides detailed images of the surface morphology of materials at high magnification and resolution. Figure (3) displays the top view of the FE-SEM images at two magnifications of 15 kx and 60 kx, displaying the surface morphologies of the PANI:PVA blend, its composite with $AgNO_3$, and its composite with $CuCl_3$. At 15 kx magnification, the FE-SEM image of the PANI:PVA blend shows a relatively smooth, nonporous, and uniform surface with minor irregularities. This smoothness indicates good blending and homogeneity between PANI and PVA. At 60 kx magnification, the image reveals more detailed surface features. Fine structures such as plate-like structures that are highly merged with the surface may be visible.

After adding $AgNO_3$, the surface appeared rougher than the pure polymer blend, with noticeable agglomerations of spherical nanoparticles highly attached to each other, forming a high-pore network with a high surface area. The $AgNO_3$ embedded in the PANI:PVA blend matrix is relatively uniform. The rougher surface with high porosity suggests an enhanced surface area and potential sites for interaction with other materials and chemicals. The embedded $AgNO_3$ nanoparticles improve the electrical conductivity and antibacterial properties, making the composite suitable for specific applications such as sensors or antimicrobial coatings. The uniform distribution of $AgNO_3$ particles is critical for ensuring consistent properties throughout the material [15].

After reinforcing with $CuCl_3$, the surface morphology exhibits significant roughness differently compared to the $AgNO_3$ composite. The detailed image reveals nanoparticles of various sizes dispersed on the smooth surface of the blend. The particles were irregular in size, which may indicate different interaction or dispersion mechanisms. The rough and clustered surface morphologies are due to increased surface area enhance catalytic and adsorption properties [9,16].

Fourier-transform infrared spectroscopy (FTIR) is a powerful technique for identifying functional groups and molecular interactions within polymers. The FTIR spectra of the PANI:PVA blend and its composites with $AgNO_3$ are shown in Fig. (4), and the corresponding band assignments are summarized in table (3).

The FTIR spectra exhibit various characteristic bands corresponding to the functional groups present in the PANI:PVA blend. The O-H stretching vibration appeared at 3414.33 $cm^{-1}$ in the PANI:PVA blend [17], with slight shifts observed in the composites with increasing $AgNO_3$ concentration, indicating possible interactions between $AgNO_3$ and the hydroxyl groups in the blend. The $CH_2$ stretching vibrations were observed at 2933.11 and 2871.67 $cm^{-1}$ [18]. The C=O stretching vibration was observed at 1710.58 $cm^{-1}$ [19]. The C=N stretching vibration was observed at 1640.96 $cm^{-1}$. The C-H bending vibration was at 1430.03 $cm^{-1}$ in the PANI:PVA blends [19], with slight shifts in this band in its composites indicating minor structural changes in the polymer blend matrix. The C-H deformation vibration was observed at 1262.12 $cm^{-1}$. The C-O stretching vibrations appeared at 1086.01 and 1049.15 $cm^{-1}$ in the PANI:PVA blend [20], with shifts in these bands in the composites implying interactions between $AgNO_3$ and the oxygen-containing groups in the polymer blend matrix. The C-C stretching vibration is at 850.51 $cm^{-1}$ [21].

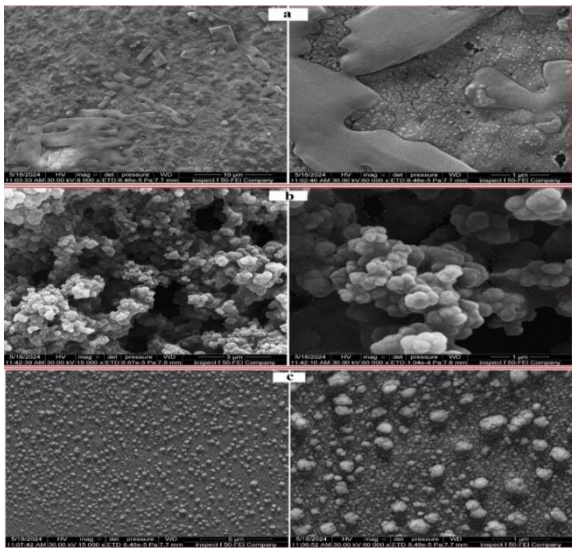


**Fig. (3) FE-SEM images of (a) PANI:PVA blend, (b) its composite with $AgNO_3$, and (c) its composite with $CuCl_3$ nanoparticles**

The incorporation of $AgNO_3$ results in shifts in the characteristic FTIR bands of the copolymers, indicating interactions between $AgNO_3$ and the functional groups in the polymer matrix. The presence of new bands in the prepared composites, specifically the Ag-O stretching vibrations at around 600 $cm^{-1}$, confirms the successful integration of $AgNO_3$ via the interaction with oxygen in the polymer. These changes in the spectra suggest modifications in the electronic environment and molecular structure of the PANI:PVA matrix, which can affect its properties for use in specific applications, such as sensors and antimicrobial coatings [22].

  

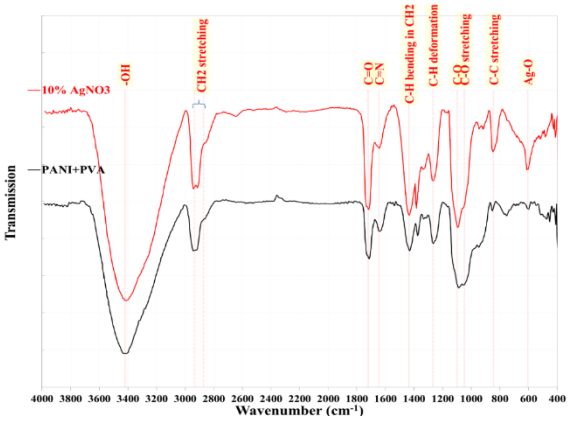


**Fig. (4) FTIR spectra of the PANI:PVA blend and its composites with $AgNO_3$ nanoparticles**

**Table (3) FTIR bands of the PANI:PVA blend and its composites with 10% $AgNO_3$ nanoparticles**

| Functional Group | Wavenumbers ($cm^{-1}$) | |
|---|---|---|
| | PANI:PVA | $AgNO_3$ nanoparticles |
| O-H | 3414.33 | 3412.29 |
| $CH_2$ | 2933.11 | 2933.11 |
| $CH_2$ | 2871.67 | 2861.43 |
| C=O | 1710.58 | 1716.72 |
| C=N | 1640.96 | 1638.91 |
| C-H bending in $CH_2$ | 1430.03 | 1434.13 |
| C-H deformation | 1262.12 | 1266.21 |
| C-O | 1086.01 | 1090.10 |
| C-O stretching | 1049.15 | 1051.19 |
| C-C | 850.51 | 846.42 |
| Ag-O | - | 602.73 |

The FTIR spectra of the PANI:PVA blend and its composites with $CuCl_3$ are shown in Figure 5. Table 4 summarizes the characteristic FTIR bands. The FTIR analysis revealed several key insights into the molecular interactions and structural modifications induced by adding $CuCl_3$ nanoparticles. The incorporation of $CuCl_3$ resulted in shifts in the characteristic FTIR bands, indicating interactions between $CuCl_3$ nanoparticles and the functional groups in the polymer blend matrix. A new band corresponding to Cu-O stretching vibration at 607.13 $cm^{-1}$ appeared in FTIR spectra. This band was absent in the PANI:PVA blend but appeared prominently in its composites, validating the formation of Cu-O interactions [13].

The appearance of new bands corresponding to Cu-O bonds indicates the successful incorporation of $CuCl_3$ into the polymer matrix, which can affect the material properties. Understanding these molecular interactions is crucial for tailoring the properties of composites for specific applications, such as sensors, conductive materials, and catalytic systems.

Some bacteria, especially Gram-negative bacteria, tend to become more antibiotic-resistant. Attention should be paid to using nanoparticles, which work by a different mechanism than traditional antibiotics [23].

The results of the antibacterial activity test of the PANI:PVA blend, and the reinforced samples with $AgNO_3$ and $CuCl_3$ nanoparticles against gram-negative and Gram-positive bacterial strains using an agar well diffusion assay are shown in figures (6) and (7). In addition, the details are explained in table (5). All samples show significant inhibition zones on the agar surface after 24 hours of incubation compared with the control sample. The diameter of the inhibitory zone indicates the degree of microorganism susceptibility. The zone range of *Escherichia coli* is greater than that of *Staphylococcus aureus* because of differences in the cell walls of the two bacterial types [24]. The activity increased after reinforcing the PANI:PVA polymer blend with $AgNO_3$ and $CuCl_3$ nanoparticles.

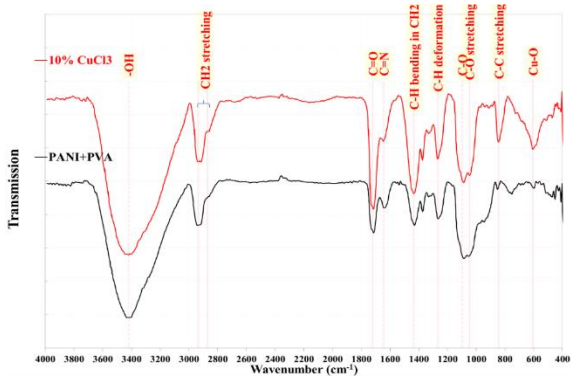


**Fig. (5) FTIR spectra of the PANI:PVA blend and its composites with $CuCl_3$ nanoparticles**

**Table (4) FTIR bands of the PANI:PVA blend and its composite with 10% $CuCl_3$ nanoparticles**

| Functional Group | Wavenumbers ($cm^{-1}$) |
|---|---|
| | $CuCl_3$ nanoparticles |
| O-H | 3420.77 |
| $CH_2$ | 2933.20 |
| $CH_2$ | 2865.38 |
| C=O | 1714.26 |
| C=N | 1648.27 |
| C-H bending in $CH_2$ | 1435.64 |
| C-H deformation | 1267.01 |
| C-O | 1087.37 |
| C-O stretching | 1045.21 |
| C-C | 843.59 |
| Cu-O | 607.13 |

The nanocomposite polymer blend displays antibacterial activity due to their stronger interaction with polysaccharides and proteins on cell walls [25]. The primary mechanism by which nanoparticles inhibit bacterial growth is the release of metal ions or reactive oxygen species from the surface of these particles [26]. The overall surface charge of *E. coli* cells is negative [5], so the binding of positive ions to the bacteria wall is caused by the electrostatic forces between the negatively charged cell walls and the positive metal ions. This causes the metal ions to accumulate on the bacteria's cell wall, causing changes in their

  

permeability, which leads to their death [27]. A few of these ions enter the cell and cause immobilization and inactivation of bacterial cells via interaction with DNA, which has a strong propensity to react with metal ions, causing degeneration that culminates in protein denaturation and cell death [28]. The results proved the possibility of using the prepared samples as antibacterial agents for surface coatings [29].

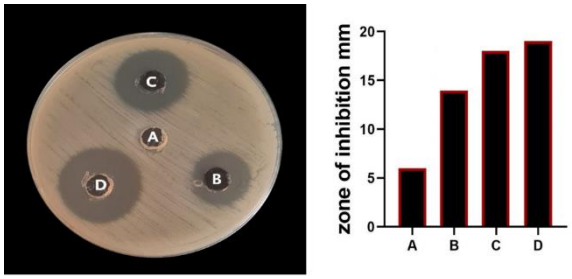


**Fig. (6) Antibacterial activity test against S. aureus. (A) Control, (B) PANI:PVA blend, (C) PANI:PVA/$CuCl_3$, and (D) PANI:PVA/$AgNO_3$**

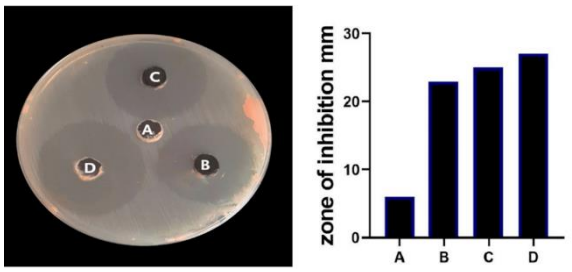


**Fig. (7) Antibacterial activity test against *E. coli.* (A) control, (B) PANI:PVA, (C) PANI:PVA/$CuCl_3$,and (D) PANI:PVA/$AgNO_3$**

**Table (4) Zone of inhibition (mm) around PANI:PVA and their composites with $CuCl_3$ and $AgNO_3$**

| Sample | PANI:PVA | PANI:PVA/ $CuCl_3$ | PANI:PVA/$AgNO_3$ |
|---|---|---|---|
| *S. aureus* | 8 | 12 | 13 |
| *E. coli* | 17 | 19 | 21 |

## 4. Conclusion

This study has successfully developed PVA/PANI nanocomposite films doped with $CuCl_3$ and $AgNO_3$ nanoparticles. The partial crystallinity and the presence of AgO and CuO phases were confirmed, indicating effective nanoparticle integration. The doping process has introduced roughness and porosity to the composite surfaces compared with the smooth surface of the pure blend. The strong molecular interactions between the nanoparticles and the polymer matrix were demonstrated. The $AgNO_3$-doped PANI nanocomposites exhibited significant inhibition against *Staphylococcus aureus* and *Escherichia coli*. These results highlight the potential of $AgNO_3$-doped PANI nanocomposites for antimicrobial applications, particularly as surface coatings.

## References

[1] K.K. Sadasivuni, D. Ponnamma, M. Rajan, B. Ahmed, and M.A.S.A. Al-Maadeed, eds., **"Polymer Nanocomposites in Biomedical Engineering"**, Lecturenotes in Bioengineering, Springer International Publishing (2019).

[2] H. Wafaa, **"Coordination Chemistry of Polyvinyl Alcohol"**, Lambert Academic Publishing GmbH (2013).

[3] M.N. Subramanian, "Polymer Blends and Composites: Chemistry and Technology", in **"Polymer Science and Plastics Engineering"**, Wiley (2017).

[4] J.R. Torrey, "Antimicrobial Properties Of Metal And Metal-Halide Nanoparticles And Their Potential Applications", University of Arizona (2014).

[5] M. Godoy-Gallardo et al., "Antibacterial approaches in tissue engineering using metal ions and nanoparticles: From mechanisms to applications", *Bioactive Mater.*, 6(12) (2021) 4470–4490.

[6] K. Jeyabanu et al., "Effect of electrical conductivity studies for CuS nanofillers mixed magnesium ion based PVA-PVP blend polymer solid electrolyte", *Physica B: Cond. Matter*, 572 (2019) 129-138.

[7] Z. Breijyeh, B. Jubeh and R. Karaman, "Resistance of Gram-Negative Bacteria to Current Antibacterial Agents and Approaches to Resolve It", *Molecules*, 25(6) (2020) 1340.

[8] D. Manyasree, P. Kiranmayi and S.N.R. Kumar, "Synthesis, Characterization and Antibacterial Activity of Aluminium Oxide Nanoparticles", *Int. J. Pharm. Pharmaceut. Sci.*, 10(1) (2018) 32.

[9] N.R. Chiou et al., "Growth and alignment of polyaniline nanofibres with superhydrophobic, superhydrophilic and other properties", *Nature Nanotech.*, 2(6) (2007) 354-357.

[10] M.F.H. Abd El-Kader et al., "Structural, morphological features, and antibacterial behavior of PVA/PVP polymeric blends doped with silver nanoparticles via pulsed laser ablation", *J. Mater. Res. Technol.*, 13 (2021) 291-300.

[11] D. Vaes and P. Van Puyvelde, "Semi-crystalline feedstock for filament-based 3D printing of polymers", *Prog. Polym. Sci.*, 118 (2021) 101411.

[12] T.-D. Nguyen et al., "Iridescent cellulose nanocrystal films: the link between structural colour and Bragg's law", *Euro. J. Phys.*, 39(4) (2018) 045803.

[13] S.V. Moharil, N.S. Bajaj and P.K. Tawalare, **"Luminescent Metal Oxides: Materials to Technologies",** CRC Press (2023).

[14] S. Ma et al., "To Study the Structural Characterization of the Polyaniline/$CoFe_2O_4$ Nanocomposites", *Int. J. Appl. Phys.*, 9(2) (2022) 1-6.

  

[15] D. Coetzee et al., "Influence of Nanoparticles on Thermal and Electrical Conductivity of Composites", *Polymers*, 12(4) (2020) 742.
[16] M. Beygisangchin et al., "Polyaniline Thin Films - A Review", *Polymers*, 13 (2021) 1–46.
[17] M.G. Hammed and A.A. Hassan, "Enhancement of the Structural and Optical Properties of (PVA-PANI) Polymer Blend by Addition of CuI Nanoparticles", in *IOP Conf. Ser.: Mater. Sci. Eng.*, 7 (2020) 928.
[18] D.B. Dupare, M.D. Shirsat and A.S. Aswar, "Metal Oxides Doped PPY-PVA Blend Thin Films", *Sens. Transd. J.*, 101(2) (2009) 82-89.
[19] M.K. Mohanapriya et al., "Influence of cerium oxide ($CeO_2$) nanoparticles on the structural, morphological, mechanical and dielectric properties of PVA/PPy blend nanocomposites", *Mater. Today: Proc.*, 3(6) (2016) 1864-1873.
[20] I.S. Elashmawi, A.M. Ismail and A.M. Abdelghany, "The incorporation of polypyrrole (PPy) in CS/PVA composite films to enhance the structural, optical, and the electrical conductivity", *Polymer Bull.*, 80(10) (2023) 11379-11399.
[21] J. Ding, Y. Li and M. Li, " Preparation of Functionalized Magnetic Polystyrene Microspheres and Their Application in Food Safety Detection", *Smart Func. Polymer*, 15(1) (2022) 77.
[22] S. H. Simon, **"The Oxford Solid State Basics",** Oxford University Press (Oxford, 2013).
[23] Inamuddin, **"Green Polymer Composites Technology: Properties and Applications",** CRC Press (2016).
[24] The Society for Applied Bacteriology, Summer Conference, *J. Appl. Bacteriol.*, 77 (1994) 1-24.
[25] V. Guarino, M. Iafisco and S. Spriano, **"Nanostructured Biomaterials for Regenerative Medicine"**, Woodhead Publishing Series in Biomaterials (Elsevier Science, 2019).
[26] A.K. Suresh, **"Metallic Nanocrystallites and Their Interaction with Microbial Systems**", SpringerBriefs in Molecular Science (Springer Netherlands, 2012).
[27] K. De Vriese et al., "Pharmacological Strategies for Manipulating Plant $Ca^{2+}$ Signalling", *Int. J. Mol. Sci.*, 19(5) (2018) 1506.
[28] X. Huangfu et al., "A review on the interactions between engineered nanoparticles with extracellular and intracellular polymeric substances from wastewater treatment aggregates", *Chemosphere*, 219 (2019) 766–783.
[29] S. Bandyopadhyay et al., "Bacterial cellulose and guar gum based modified PVP-CMC hydrogel films: Characterized for packaging fresh berries", *Food Pack. Shelf Life*, 22 (2019) 100402.

**Table (2) XRD parameters of the PANI:PVA/$AgNO_3$ composite.**

| 2θ (Deg.) | FWHM (Deg.) | $d_{hkl}$ Exp.(Å) | D (nm) | Phase | hkl | Card No. |
|---|---|---|---|---|---|---|
| 20.2832 | 0.2787 | 4.3747 | 29.0 | $AgNO_3$ | (111) | 01-084-0713 |
| 21.6150 | 0.3717 | 4.1080 | 21.8 | $AgNO_3$ | (200) | 01-084-0713 |
| 24.1239 | 0.3097 | 3.6862 | 26.2 | $AgNO_3$ | (111) | 01-084-0713 |
| 29.6372 | 0.4646 | 3.0118 | 17.7 | $AgNO_3$ | (200) | 01-084-0713 |
| 31.9912 | 0.4337 | 2.7954 | 19.1 | $AgNO_3$ | (111) | 01-084-0713 |
| 32.5796 | 0.4027 | 2.7462 | 20.6 | $AgNO_3$ | (200) | 01-084-0713 |
| 37.6100 | 0.3100 | 2.3880 | 25.9 | Mono. AgO | (111) | 96-900-8963 |
| 54.4210 | 0.3300 | 1.6850 | 22.9 | Mono. AgO | (31-1) | 96-900-8963 |

**Table (2) XRD parameters of the PANI:PVA/$CuCl_3$ composite.**

| 2θ (Deg.) | FWHM (Deg.) | $d_{hkl}$ Exp.(Å) | D (nm) | hkl | Card No. |
|---|---|---|---|---|---|
| 35.3166 | 0.2678 | 2.5394 | 31.1 | (11-1) | 96-101-1195 |
| 38.8270 | 0.3273 | 2.3175 | 25.7 | (111) | 96-101-1195 |
| 45.0744 | 0.2083 | 2.0097 | 41.3 | (-112) | 96-101-1195 |
| 48.9120 | 0.4165 | 1.8607 | 21.0 | (20-2) | 96-101-1195 |
| 57.8071 | 0.8032 | 1.5937 | 11.3 | (202) | 96-101-1195 |
| 61.6447 | 0.4760 | 1.5034 | 19.4 | (-113) | 96-101-1195 |

  